Stochastic modelling of surface texture generated by high-energy jets

R Kovacevic, BS, MS, PhD, SME, **R Mohan,** BS, MS, SME
Center for Robotics and Manufacturing Systems and Department of Mechanical Engineering, University of Kentucky, Lexington, Kentucky, USA

Y M Zhang, BS, MS, PhD
Harbin Institute of Technology, Harbin, People's Republic of China

The surfaces produced by two different jet cutting processes, namely abrasive waterjet (AWJ) cutting and laser machining, are characterized for a comparative study. The surface profile measurements from experiments are modelled using auto regressive moving average (ARMA) models. The characteristics of the different profiles are identified by analysing these models. To describe the surface adequately, a sufficiently large sized sample is utilized for modelling. A novel method for identifying ARMA models based on the concept of model distance, which is ideal for large size samples, is adopted here. The relative advantages of this method are quantified in terms of the accuracy ratio. The profile characteristics (both dynamic as well as static) reveal more information about the nature of these processes. Scanning electron microscope (SEM) photographs of the surfaces generated by laser and AWJ are analysed to obtain more insight into the physics of these processes.

1 INTRODUCTION

Jet cutting processes like abrasive waterjet (AWJ), laser and plasma arc cutting are being used more and more for cutting difficult-to-machine materials. These jet cutting processes have been found to be very effective in areas where conventional cutting processes are difficult to implement. The jet cutting operations can be broadly classified into cold jet cutting processes and hot jet cutting processes. Waterjet cutting and AWJ cutting belong to the former, whereas laser cutting and plasma arc cutting fall under the latter category. In order to achieve the desired surface finish, these jet cutting processes need to be controlled. Characterization of the surface profiles gives us information about how to control the processes.

The surface profiles obtained by different manufacturing processes can be characterized using various methods. The height distribution of the surface profile of any machined surface can be satisfactorily represented by asperity functions like roughness average (R_a) or r.m.s. roughness (R_q) or maximum peak-to-valley height (R_t). The third and fourth central moments, namely skewness (R_{sk}) and kurtosis (R_{ku}), can be used to represent the shape of the surface profile distribution about the mean. However, jet cutting processes produce surfaces with repetitive striations. In order to characterize the repetitive shape of the profile by combining the height distribution and spatial characteristics, stochastic models obtained by time series analysis will be preferred.

Various methods have been adopted for characterization of engineering surfaces either through surface profile height description or stochastic model description (**1–5**). The mechanism of striation formation on the AWJ cut surface was investigated by mathematical modelling (**6**) and through surface texture and surface integrity analysis (**7**). On-line monitoring of the AWJ cut surface was investigated (**8–10**) by developing a mathematical relationship between cutting parameters and surface roughness (R_a). Several studies were conducted to optimize the AWJ surface finish through the force feedback technique (**11–14**). By stochastic modelling, the role of cutting parameters in surface formation has been investigated (**15–18**). From these studies, it can be seen that stochastic model characterization has provided an insight into the cutting processes. In this paper, laser cut surfaces will also be in the scope of study. There have been several investigations (**19–21**) on the characterization of the laser cut surface through surface profile height distribution.

Although stochastic models have been used to characterize the surfaces cut by AWJ, laser cut surfaces have been characterized through height distribution only. Moreover, no comparative studies have been performed. Also, in previous modelling of surfaces, data sets having only a few hundred observations have been utilized to fit auto regressive moving average (ARMA) models due to the extensive computational burden of conventional modelling approaches. Inaccurate models are frequently obtained. Thus, in this study, model comparison and accuracy become the primary interests.

The present authors have proposed a novel ARMA modelling approach to sufficiently employ extensive data to improve accuracy (**22**) based on the concept of model distance. This method will be used to identify ARMA models in this paper. The relative advantages of this method will be discussed in Section 4. The samples are cut at different cutting speeds which is the common predominant factor influencing the surface characteristics of both jet cutting processes. The workpiece is copper with ceramic coating (the coating thickness is approximately 0.050 mm), a composite material of thickness 1.65 mm used as the printed circuit board for surface mount devices. A comparative study of the scanning electron micrographs (SEM) of the surfaces generated by laser and AWJ reveal more information about

The MS was received on 2 September 1992 and was accepted for publication on 25 February 1993.

0954-4054/93 $3.00 + .05

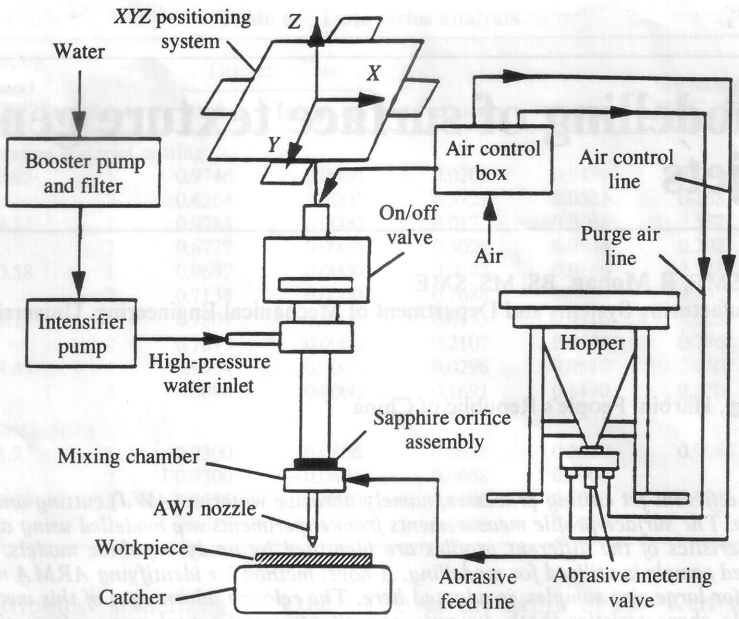

Fig. 1 Schematic of abrasive waterjet cutting system

the physics of these processes. The SEM of sheared surface and surface produced by bandsaw cutting are also given for comparison.

2 EXPERIMENTAL SET-UP AND PROCEDURE

The first phase of the experimental study is conducted using an AWJ cutting system consisting of a high-pressure intensifier pump, AWJ cutting head, abrasive metering and delivery system, catcher tank and *XYZ* positioning table controlled by a computerized numerical control (CNC) controller. A schematic of the AWJ cutting system is shown in Fig. 1. Constant process parameters for AWJ cutting are given in Table 1.

The second phase is conducted using a laser machining system. A schematic of the laser machining system is shown in Fig. 2. It consists of a laser beam generation system, a beam delivery system, workpiece positioning system and auxiliary devices. An Nd/YAG laser which has a wavelength of 1.06 μm is good for cutting most metals as it couples with metals very effectively. Since the workpiece base material is copper, a gas-assisted (O_2 assisted) Nd/YAG laser is used. Constant process parameters for laser cutting are given in Table 2.

Table 1 Constant process parameters for AWJ cutting

Waterjet pressure	262 MPa
Water orifice diameter	0.254 mm
Stand-off distance	8 mm
Abrasive flowrate	5.76 g/s
Abrasive type	Garnet
Abrasive size	80 mesh (0.180 mm)
Mixing nozzle length	76.2 mm
Mixing nozzle diameter	0.762 mm

Different samples were cut by AWJ and laser for a length of about 25 mm by varying the cutting speed. The profile of the cut surface was measured using a profilometer. To eliminate the effects of the entry stage and exit stage of the cutting process, the surface profile is measured at the middle of the cut for a length of about 8 mm. The data files used for laser and AWJ cuts in

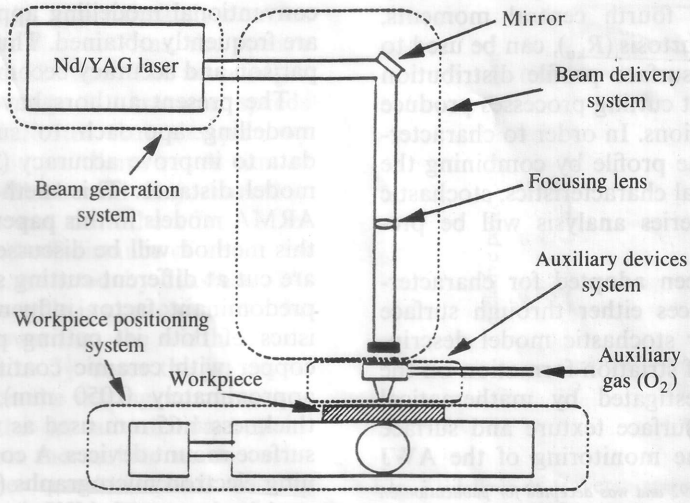

Fig. 2 Schematic of laser machining system

Table 2 Constant process parameters for laser cutting

Type of laser	Nd/YAG
Power of laser	200 W
Focus lens	150 mm
Mode of operation	Pulsed wave
Pulsing frequency	40 Hz
Secondary gas used	O_2
Secondary gas pressure	0.414 MPa
Orifice diameter	1.524 mm
Stand-off distance	0.8 mm

reference (**23**) (except one) are adopted here for analysis. ASCII file is generated from the data file of the cut profile using a suitable data exchange protocol. Surface roughness parameters like R_a, skewness and kurtosis are measured to quantify the static characteristics of the surface profile.

The ASCII file consisted of about 4480(N) observations per measurement with a sampling interval of 1.25 μm. The number of data points (per data set) used here is much larger than that used for similar work in this area, which is of the order of 350 (**18**) only. Each data set is fitted using suitable ARMA models. Even though ARMA modelling has been verified to be an effective tool for characterization of various engineering surfaces, there is no suitable approach for selecting an optimum interval for ARMA characterization. Furthermore, the accuracy requirement varies from case to case. Hence, more data are expected to be processed for more accurate results. The problem is that the computational burden prevents one from selecting extensive data. As a matter of fact, since the parameter estimation of the ARMA models is non-linear, and since the computational burden of the conventional methods [for example, the non-linear least squares (NLS) method (**24**) and maximum likelihood (ML) method (**25**)] is proportional to the sample sizes, the identification of large samples will be time consuming. Therefore, an alternative algorithm for identifying ARMA models has been proposed (**22**) based on the concept of model distance.

The concern of this approach is to decrease the computational burden to accuracy ratio with reliable evaluation of the final modelling accuracy, for surface modelling. The procedure for the proposed approach consists of two steps: (a) identifying an AR model from the samples (AR modelling); (b) identifying the ARMA model based upon this AR model (ARMA approximation). The flow chart in Fig. 3 gives the outline of this procedure. Details of this procedure are available in reference (**22**). It has been shown that, by this method, the modelling accuracy to computational burden ratio increases with sample size, whereas this ratio in conventional methods is nearly constant. Also, its computational burden is nearly independent of the sample size. This makes it possible to adequately utilize extra samples to improve the modelling accuracy without a virtual increase in the computational burden. In this paper, this approach will be used to identify the ARMA models. The benefits of utilization of this approach will be discussed in Section 4.

Using SEM, the cut surfaces are photographed and the observations are analysed. Higher magnification ($\times 500$) of the interface of the composite layers is chosen for SEM to better understand the phenomenon of delamination associated with the jet cutting processes.

3 RESULTS AND DISCUSSION

Surface roughness parameters measured for different profiles are given in Table 3. The surface roughness parameters for shearing and bandsaw cutting are given for comparison. The plots of surface roughness (R_a) versus cutting speed for AWJ and laser are shown in Fig. 4.

It can be seen that, within each process, R_a increases with an increase in the cutting speed. The cut produced by the jet at an instance overlaps with the previous cut as the cut progresses. This has a tendency to smooth the surface. The jet overlap can be considered to be a function of the cutting speed as well as steps per input unit of the positioning system. Steps per input unit remaining constant, the jet overlap decreases with an increase in cutting speed, making the surface rougher. This reasoning can be supported by the trend noticed in the value of R_{ku} (at speeds above 4.23 mm/s) with an increase in cutting speed for AWJ cutting. It can be noticed that at higher cutting speeds the laser cutting produces a very rough surface compared to the AWJ cutting. This can be attributed to the fact that a laser has a heating effect on the material being cut (evident in the SEM photographs). As a result, the material melts and loses its surface texture when it becomes resolidified. In order to ensure through cutting, the laser cutting has to be much slower than AWJ cutting. It can also be noticed that R_{sk} is approximately equal to zero and R_{ku} is approximately equal to three for both jet cutting processes (which is typical of a pure Gaussian shape). From the values of R_{sk} and R_{ku} obtained, it can be concluded that the surface profile is predominantly Gaussian in nature. A similar observation was made by Query *et al.* (**26**) for a laser cut surface.

The surface profiles obtained are described by the following ARMA(p,q) model (**25**):

$$Y_t - \Phi_1 Y_{t-1} - \Phi_2 Y_{t-2} - \cdots - \Phi_p Y_{t-p} = a_t - \Theta_1 a_{t-1} - \Theta_2 a_{t-2} - \cdots - \Theta_q a_{t-q} \quad (1)$$

where

Y_t is the height of the profile at a distance t and $a_t \sim \text{NID}(0, \sigma_a^2)$.

Using the model distance based method ARMA models of orders ranging from (4,3) to (2,1) were obtained. Out of seven cases, ARMA(2,1) was found to

Table 3 Surface roughness parameters

Cutting speed mm/s	R_a μm	R_{sk}	R_{ku}
Abrasive waterjet cutting			
0.85	3.2282	0.0524	3.2370
4.23	3.9873	−0.1879	2.9502
10.58	4.6294	−0.1351	3.1927
21.17	4.6770	−0.1942	3.4151
44.45	6.2116	0.2772	3.5197
Laser cutting			
1.27	5.1272	0.4222	3.5736
3.39	22.8154	0.0123	3.5152
Shearing			
—	301	−0.0250	3.8930
Bandsaw cutting			
—	12.2494	−0.0213	2.8222

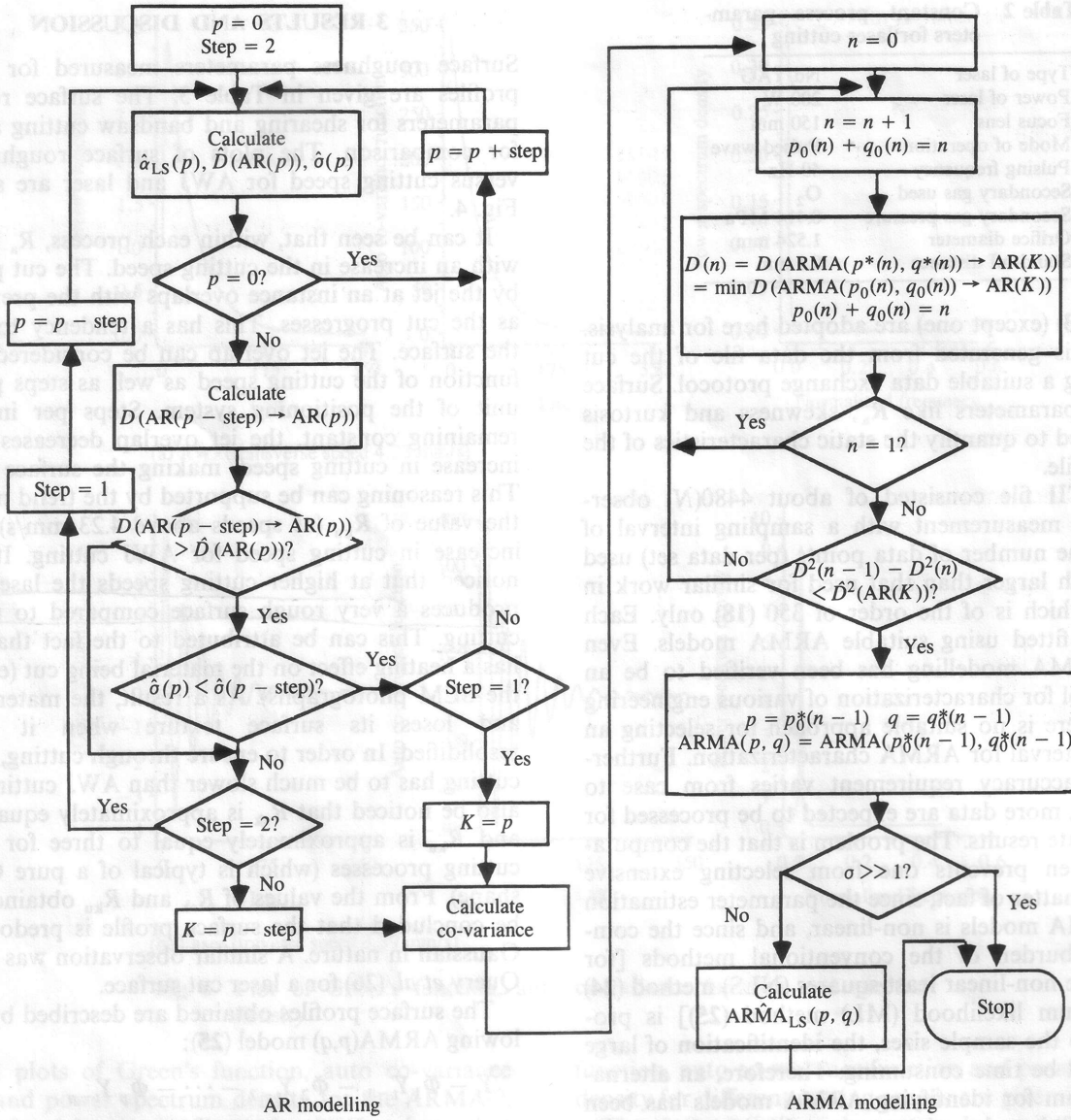

$\hat{\alpha}_{LS}(p)$ parameter estimate vector of AR(p)
$\hat{\sigma}(p)$ standard deviation estimate of AR(p) modelling residual
$\hat{D}$(AR(p)) parameter estimate error (measured in the model distance)
$D(M_1 \rightarrow M_2)$ model distance from M_1 to M_2
AR(K) selected AR model

Fig. 3 Flow chart to show the procedure of ARMA modelling by model distance

represent adequately the data for six cases. One case was represented by ARMA(4,3). Hence, each set of data was fitted with ARMA(2,1) for uniform comparison. Green's function (impulse response function), auto co-variance function and power spectrum density are obtained from the fitted ARMA(2,1) model.

The ARMA(2,1) model obtained for AWJ cutting and laser cutting can be represented by the general equation

$$Y_t = \Phi_1 Y_{t-1} + \Phi_2 Y_{t-2} + a_t - \Theta_1 a_{t-1} \qquad (2)$$

where

Y_t and a_t are as given above.

The parameters of the ARMA(2,1) models obtained are given in Table 4. From this table it can be seen that as the traverse speed increases, the variance (σ_a^2) increases for both AWJ as well as laser cutting (with

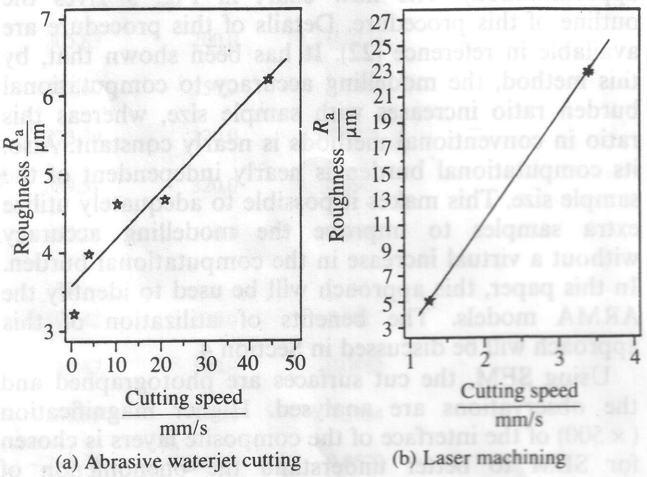

(a) Abrasive waterjet cutting (b) Laser machining

Fig. 4 Plot of surface roughness versus cutting speed

Table 4 Parameters of ARMA(2,1) models

Cutting speed mm/s	Φ_1	Φ_2	Θ_1	σ_a
Abrasive waterjet cutting				
0.85	1.601	−0.6105	−0.2335	0.0325
4.23	1.656	−0.6630	−0.2616	0.0424
10.58	1.683	−0.6917	−0.2104	0.0470
21.17	1.748	−0.7525	−0.1160	0.0475
44.45	1.772	−0.7790	−0.1887	0.0695
Laser cutting				
1.27	1.860	−0.8714	0.2501	0.0427
3.39	1.925	−0.9652	−0.0399	0.2822

one exception). This gives an indication about the effect of the traverse speed on the dynamic response of the system.

Green's function for an ARMA(2,1) model is given by (**24**)

$$G_j = g_1\lambda_1^j + g_2\lambda_2^j = \left(\frac{\lambda_1 - \Theta_1}{\lambda_1 - \lambda_2}\right)\lambda_1^j + \left(\frac{\lambda_2 - \Theta_1}{\lambda_2 - \lambda_1}\right)\lambda_2^j \quad (3)$$

where j is the lag and λ_1 and λ_2 are the characteristic roots of the model.

The variance decomposition for each root of the ARMA(2,1) model is given by

$$d_1 = \frac{g_1^2}{1-\lambda_1^2} + \frac{g_1 g_2}{1-\lambda_1\lambda_2} \quad (4)$$

$$d_2 = \frac{g_1 g_2}{1-\lambda_1\lambda_2} + \frac{g_2^2}{1-\lambda_2^2} \quad (5)$$

The auto co-variance function γ_k defines the dependence of Y_t on Y_{t-j} (**24**). It is expressed by

$$\gamma_j = d_1\lambda_1^j + d_2\lambda_2^j \quad (6)$$

The power spectrum density function which is the transform of the auto co-variance function is given by (**25**)

$$g(f) = 2\sigma_a^2 \frac{|1 - \theta_1 e^{-i2\pi f}|^2}{\gamma_0 |1 - \Phi_1 e^{-i2\pi f} - \Phi_2 e^{-i4\pi f}|^2} \quad (7)$$

where $0 \leqslant f \leqslant \frac{1}{2}$.

The spectral density from the original profile and that from the ARMA(2,1) model representing the surface cut by abrasive waterjet at a traverse speed of 10.58 mm/s are given in Fig. 5a and b respectively as a typical example. Figure 5c gives the surface profile generated from the original data. It can be seen that the spectral density from the model very closely resembles that from the original profile. They almost overlap each other.

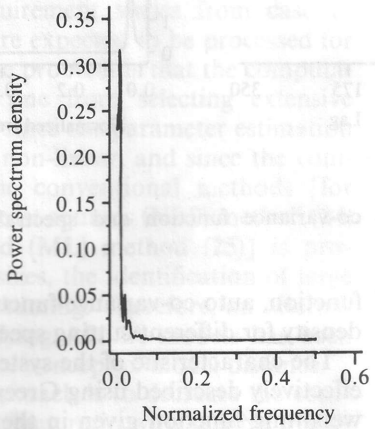

(a)

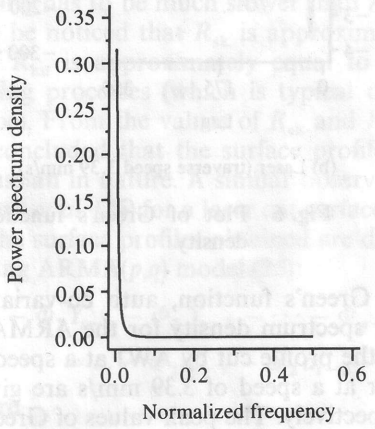

(b)

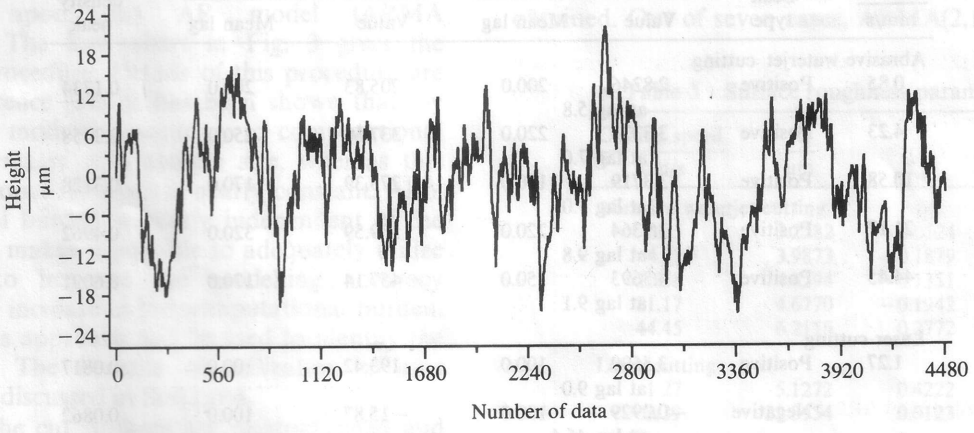

(c)

Fig. 5 (a) Spectral density from original profile
(b) Spectral density from model
(c) Surface profile from original data (AWJ speed 10.58 mm/s)

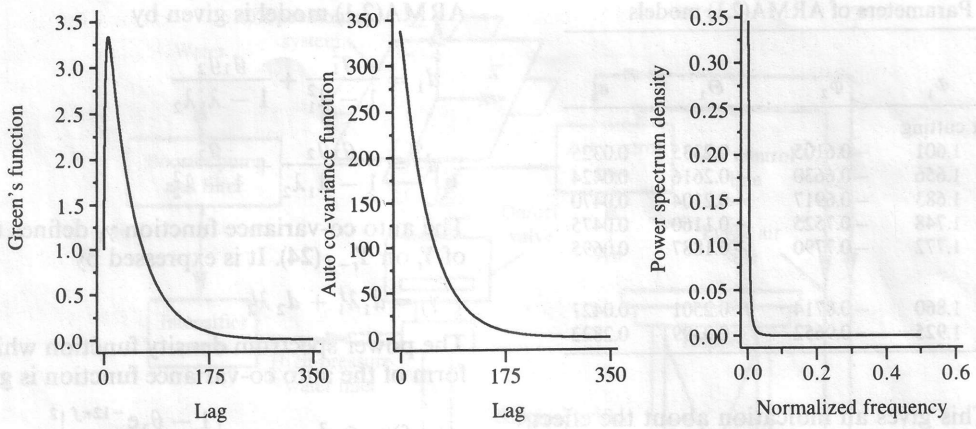

(a) AWJ (transverse speed 4.23 mm/s)

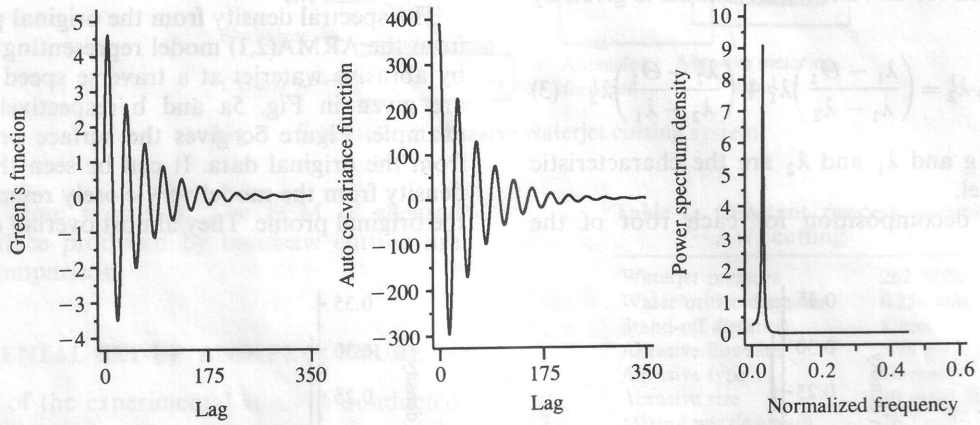

(b) Laser (traverse speed 3.39 mm/s)

Fig. 6 Plot of Green's function, auto co-variance function and spectral density

Typical plots of Green's function, auto co-variance function and power spectrum density for the ARMA(2, 1) models fitted for the profile cut by AWJ at a speed of 4.23 mm/s and laser at a speed of 3.39 mm/s are given in Fig. 6a and b respectively. The peak values of Green's function, auto co-variance function and power spectrum density for different cutting speeds are given in Table 5.

The characteristic of the system dynamics can be very effectively described using Green's function (G_j). It is the weighting function given in the present response to the

Table 5 System dynamics

Cutting speed mm/s	Peak type	Green's function Value	Green's function Mean lag	Auto co-variance function Value	Auto co-variance function Mean lag	Spectrum density peak
Abrasive waterjet cutting						
0.85	Positive	2.8246 at lag 5.8	200.0	205.83	200.0	0.1734
4.23	Positive	3.3323 at lag 7.0	220.0	337.60	250.0	0.3458
10.58	Positive	3.3719 at lag 7.0	190.0	273.39	170.0	0.3128
21.17	Positive	3.9364 at lag 9.8	220.0	559.59	320.0	0.4962
44.45	Positive	4.3693 at lag 9.1	150.0	457.14	170.0	0.6091
Laser cutting						
1.27	Positive	3.5699 at lag 9.0	100.0	193.42	100.0	0.0817
	Negative	−0.2929 at lag 45.4	100.0	−15.87	100.0	0.0862
3.39	Positive	4.6141 at lag 6.4	340.0	389.89	340.0	0.2734
	Negative	−3.5025 at lag 22.0	340.0	−295.96	340.0	9.0620

shock or disturbance a_t that is caused j-time units back (**24**). It can also be said that Green's function denotes how well the system remembers the previous shocks. On seeing the typical plots of Green's function of the AWJ cut surface (Fig. 6a) it can be concluded that the roots of the model are real. From Table 5, it can be seen that, for the AWJ profile, as the cutting speed increases, the peak value of Green's function also increases. It can also be seen that, as the speed increases, the lag to reach the peak increases. However, the lag to reach the mean remains constant between 190 and 220 initially, but at higher speeds it decreases. This means that at higher speeds, even though the system takes more time to reach the peak, it stabilizes at the mean faster. These phenomena suggest that traverse speed has a considerable influence on the dynamic response of the system. The disturbance caused by higher traverse speeds seems to be remembered for a less duration of time and is indicated on the surface profile. However, the disturbance caused in the recent past has a more pronounced effect on the surface profiles at higher traverse speeds than at lower speeds.

It is evident from Green's function of the ARMA(2,1) model of the laser cut surface profile (Fig. 6b) that the characteristic roots of the models are complex in nature. The peak value of Green's function, both positive and negative, increases as the traverse speed increases. It can also be seen that as the speed increases, the lag to reach the peak values of Green's function reduces. Moreover, as the speed increases the lag to reach the mean position increases considerably. Thus, at higher traverse speeds the disturbance caused in the recent past has a more pronounced effect on the surface profile. It reaches its peak faster. Also, the disturbance caused by higher traverse speeds is remembered for a longer time and is indicated on the profile. This difference in trend compared to the response of the AWJ cut surface can be attributed to the basic mechanism of laser cutting.

It is known that in fusion cutting by laser, the material is melted at the erosion front and ejected from the kerf with the help (in the present case) of a reactive gas (oxygen). The temperature gradient is the most important factor influencing the cut edge quality. The larger the temperature gradient from the cut kerf to the sides, the smaller the heat affected zone (HAZ) and the thinner the layer of molten and resolidified material appearing on the sides of the cut kerf. This temperature gradient is assisted by the presence of secondary gases like O_2. Experimental results (**20**) show that when cutting rates close to the maximum obtainable are applied, the spark shower from the laser cutting kerf emerges under large angles, indicating a two-dimensional melt flow around the laser beam in the kerf. At lower cutting rates, the melt flow is predominantly one dimensional, indicated by a spark shower that emerges straight down under the cutting front. The presence of this two-dimensional melt flow and resolidified material at higher cutting rates account for such high surface roughness. (The presence of resolidified materials and impurities can be clearly seen in the SEM photographs.) The same reason can be attributed to the above difference in the trend of Green's function. Laser cutting at higher speeds leads to very narrow kerf width, resulting in rewelding of the cut surfaces. Hence, laser cutting could not be conducted at higher speeds. This is in contradiction to the observations made by Powell *et al.* (**21**) on their study on mild steel using a CO_2 laser. Powell concluded that kerf width of the laser cut was not affected by any of the process parameters. The difference in workpiece material and laser type can be the cause for this contradiction.

The auto co-variance function denotes the dependence of Y_t on Y_{t-k}. It can be shown that (**24**) Green's function is really the essence of the auto co-variance function. For the ARMA models the dynamics and the auto co-variance represent the same phenomenon, namely the memory or the dependence of an observation to the preceding observations in a time series. However, the variance decomposition of the model provides the weighting function to be given to the exponential dynamic mode of each root. From the variance decomposition of the real roots of the model representing the AWJ cut profile, it can be seen that the minor root has a negative contribution to the power of the system. The variance decomposition of the complex roots related to the laser cut profile indicate that both roots have equal weights and the roots, being in conjugate pairs, give an exponentially decaying sinusoidal mode to the system dynamics.

Knowledge of the auto co-variance function is mathematically equivalent to the knowledge of spectrum and vice versa (**25**) as the power spectrum is the Fourier cosine transform of the auto co-variance function. However, the spectral density function is used to define the spectrum based on auto co-relation rather than the auto co-variances. Hence, spectral density sheds light on a different but equivalent aspect of the series. From the power spectrum density of the AWJ cut profile it is very clear that low frequencies are more predominant. This predominance increases with an increase in traverse speed (with one exception) denoted by the peak value of the spectral density. The power spectrum density of the laser cut profile indicates the presence of the complex characteristic root, shown by the shift in its peak value.

Thus, it can be seen that Green's function characterizes the ARMA models from a systems point of view. It is independent of the nature of the input. Green's function can be considered as a transfer function that transforms the input a_t into the output Y_t by (**24**)

$$Y_t = \frac{\Theta(B)}{\Phi(B)} a_t \tag{8}$$

irrespective of whether the input a_t is deterministic or stochastic. Once the basic co-variance structure of the input a_t is defined, it is Green's function that completely determines the auto co-variance structure of the output Y_t. In other words, given the input a_t, the dynamic response or output is given by its 'convolution' with Green's function. Similarly, given the co-variance of the input, the auto co-variance of the output is given by its 'double convolution' with Green's function. Also, the auto co-variance function gives the variance decomposition of the model. The power spectrum density gives information about the dynamic response of the system in the frequency domain. Thus, it can be concluded that Green's function, auto co-variance function and power spectrum density are very useful tools in representing the dynamic characteristics of a system and each one of

Table 6 Time series analysis

Cutting speed		Discrete roots				Wavelength
mm/s	Root	Real	Imaginary	Frequency	Power	mm
Abrasive waterjet cutting						
0.85	1	0.9746	0.0000	0.0205	0.9479	3.049
	2	0.6264	0.0000	0.3722	0.0521	0.168
4.23	1	0.9783	0.0000	0.0175	0.9466	3.577
	2	0.6777	0.0000	0.3096	0.0534	0.202
10.58	1	0.9697	0.0000	0.0245	0.9166	2.548
	2	0.7134	0.0000	0.2688	0.0834	0.233
21.17	1	0.9807	0.0000	0.0155	0.9316	4.022
	2	0.7673	0.0000	0.2107	0.0684	0.296
44.45	1	0.9634	0.0000	0.0296	0.8510	2.110
	2	0.8086	0.0000	0.1691	0.1490	0.370
Laser cutting						
1.27	1	0.9300	0.0806	0.0688	0.5000	0.9083
	2	0.9300	−0.0806	0.0688	0.5000	
3.39	1	0.9625	0.1970	0.1606	0.5000	0.3891
	2	0.9625	−0.1970	0.1606	0.5000	

these characteristics contributes something to the understanding of the stochastic process, due to their representational value.

The characteristic roots of each ARMA(2,1) model obtained and the wavelength decomposition of the models are given in Table 6. This table also gives the pseudo-frequencies and relative powers of the roots. We can see that the model of the AWJ profile has real roots whereas the model of laser cutting has complex roots, both being asymptotically stable.

The percentage contribution of each characteristic root to the total variance of the data is given by the relative power. It can be seen that the primary (larger) root leads to the larger wavelength and hence larger power. The secondary root contributes to minor power and smaller wavelength. Power for this major root reached 92 per cent in most of the cases of AWJ cuts. This secondary wavelength has a damping (smoothing) effect on the profile compared to the primary wavelength, as its variance is negative in nature. It is evident that the major (primary) wavelength does not change significantly up to a traverse speed of 21.17 mm/s. Tan (**6**) has hypothesized that the major wavelength represents the influence of the AWJ stream on the surface. In the present case, the mixing nozzle diameter was 0.762 mm. It can be shown that the waterjet stream diverges immediately upon exit from the mixing nozzle. The effective diameter of the jet approximately doubles over the stand-off distance of 8 mm. Thus, the stream width will be approximately 1.524 mm. The wavelength decomposition of the cuts made for traverse speeds from 0.85 to 21.17 mm/s indicates that the primary wavelength is about twice the jet diameter. A similar observation was made by Webb and Rajurkar (**15**). (However, their assumption was that the effective jet diameter doubles over a stand-off distance of about 1.6 mm.) Visualization studies conducted by Hashish (**27**) indicate that the width of one cycle is approximately the jet diameter. Tan (**6**) has shown that the width of one cycle is approximately equal to $2\frac{1}{2}$ times the jet diameter. The relationship between the mixing nozzle diameter and the diameter of the jet at various cutting conditions and their effect on the surface needs to be investigated further. At higher traverse speeds (speeds above 21.17 mm/s) the effective jet diameter reduces over the depth of cut. Kerf width taper, which is very predominant at higher traverse speeds, can be attributed as the cause for the reduction in the primary wavelength at higher speeds.

The wavelength decomposition corresponding to the lower power and minor root (secondary wavelength) can be considered to represent the abrasive mesh size. The secondary wavelength of the roots is approximately the same as the abrasive size of 0.18 mm up to a traverse speed of 21.17 mm/s. The steadiness (or unsteadiness) of motion of the AWJ traverse system is another factor that influences the surface profile significantly (**7**). At speeds higher than 21.17 mm/s, its effect is more pronounced, making the secondary wavelength different from the abrasive mesh size. The effect of traverse speed on the relative power of the primary root of ARMA(2,1) models for AWJ cut surfaces is given in Fig. 7. It can be easily seen that the relative power of the secondary root of the model behaves opposite to that of the primary root.

Existence of a single wavelength for the ARMA(2,1) model representing the surface profile generated by the laser cutting can be assumed to indicate that the flow of the laser and the assisted gas are the only factors that influence the profile. At a traverse speed of 1.27 mm/s

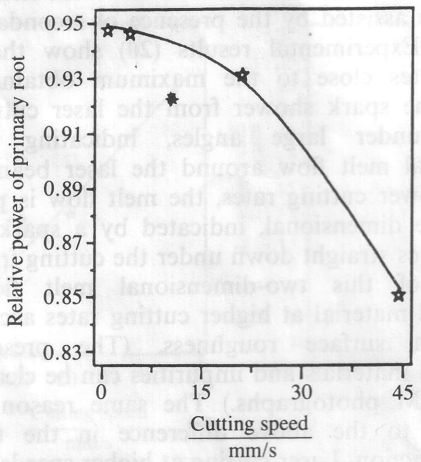

Fig. 7 Effect of traverse speed on relative power of primary root (AWJ)

the melt flow is one dimensional in nature. The wavelength of the model is observed to be about two-thirds of the assist gas orifice diameter. This is in contradiction to the observation in reference (**23**). Hence, it can be concluded that the wavelength of the laser profile model does not have a simple relationship with the assist gas orifice diameter. For a traverse speed of 3.39 mm/s the wavelength of the laser machined surface profile is only 0.3891 mm. This could be attributed to the two-dimensional flow of molten metal at such high speeds. The assist gas is not in a position to eject the molten metal at this cutting speed (maximum speed obtainable to ensure through cutting).

4 ANALYSIS OF THE MODEL DISTANCE (MD) APPROACH

The advantages of using the MD approach is twofold: one is in terms of the improvement in the modelling accuracy and the other is in terms of saving in the computational burden. It can be seen that (**22**) both the computational burden as well as modelling accuracy have been related to the size of the samples and the number of parameters. However, the benefit of this approach is that its computational burden is independent of the sample size, while for conventional algorithms the computational burden is proportional to the sample size. Hence, the extra large samples available can be conveniently used to increase the modelling accuracy without an increase of the computational burden. Thus, the benefit offered by this approach is quantified in terms of the accuracy ratio of this algorithm to the non-linear least squares (NLS) algorithm.

The minimum sample size that ensures the same accuracy to the computational burden ratio between the model distance method and the NLS algorithm can be defined as the beneficial sample size N_b given by (**22**) the equation

$$N_b = \frac{8K_m(K+5)^2}{(p+q)(p+3q+4)} \tag{9}$$

where p and q are the orders of the best fit ARMA model, $K_m(=30)$ is the maximum possible order of the adequately accurate finite-order AR approximation to the infinite AR model and K is the order of the best-fit AR model.

Let N be the sample size of the data set used for modelling in the MD based algorithm. The accuracy ratio σ of the MD algorithm to the NLS algorithm is given by

$$\sigma = \frac{N}{N_b} \tag{10}$$

Table 7 shows that the approach of the model distance criterion provides much more accurate ARMA models of surface profile data than the non-linear least squares method. This table also gives the model distance, D, between the ARMA models obtained through the MD approach and the respective models of the NLS approach.

5 SCANNING ELECTRON MICROSCOPY (SEM)

The physics of the jet cutting processes can be further studied by comparing the scanning electron microscope (SEM) photographs of the cut surfaces. A comparative study of the SEM photographs will also yield more insight into the variation in the quality of the surfaces generated by different processes. A magnification of 50 was chosen initially for all the surfaces for uniform comparison. The SEM photographs are given in Fig. 8a to i.

The SEM photograph of the laser cut surface (Fig. 8b) very clearly shows the presence of resolidified molten material. The blackened copper surface is clearly seen on the surface cut at a traverse speed of 3.39 mm/s, indicating that the heat affected zone is thicker than at the surface cut at 1.27 mm/s. The bottom of the surface is seen to be rougher than the top. The ceramic surface layer particles are found as inclusions in the resolidified molten copper base. These inclusions are more for the surface cut at 3.39 mm/s. Burrs are seen on both surfaces. Ceramic layer peel-off at edges is more predominant for the surface cut at 3.39 mm/s. Pitted holes and bubbles are seen on the surface cut at 3.39 mm/s. The cut surface orientation is very random for this surface. This can be attributed to the presence of two-dimensional melt flow during cutting and subsequent

Table 7 Model comparison

Cutting speed mm/s	Sample size N	K	Models from MD method ARMA(2,1)	Models from NLS method ARMA(2,1)	N_b	σ	D^2
Abrasive waterjet cutting							
0.85	4480	4	1.6010, −0.6105 −0.2335	1.6069, −0.6121 −0.2385	720	6.20	2.6E−04
4.23	4480	4	1.6560, −0.6630 −0.2616	1.6511, −0.6581 −0.2704	720	6.20	5.3E−05
10.58	4480	4	1.6830, −0.6917 −0.2104	1.6296, −0.6342 −0.2839	720	6.20	7.3E−03
21.17	4480	6	1.7480, −0.7525 −0.1160	1.7363, −0.7381 −0.1626	1076	4.17	4.6E−03
44.45	4480	3	1.7720, −0.7790 −0.1887	1.7692, −0.7719 −0.1926	569	7.88	6.0E−03
Laser cutting							
1.27	4480	8	1.8600, −0.8714 0.2501	1.8000, −0.8016 0.1817	1502	2.98	3.8E−02
3.39	4480	3	1.9250, −0.9652 −0.03988	1.7703, −0.7719 −0.3007	569	7.88	6.4E−01

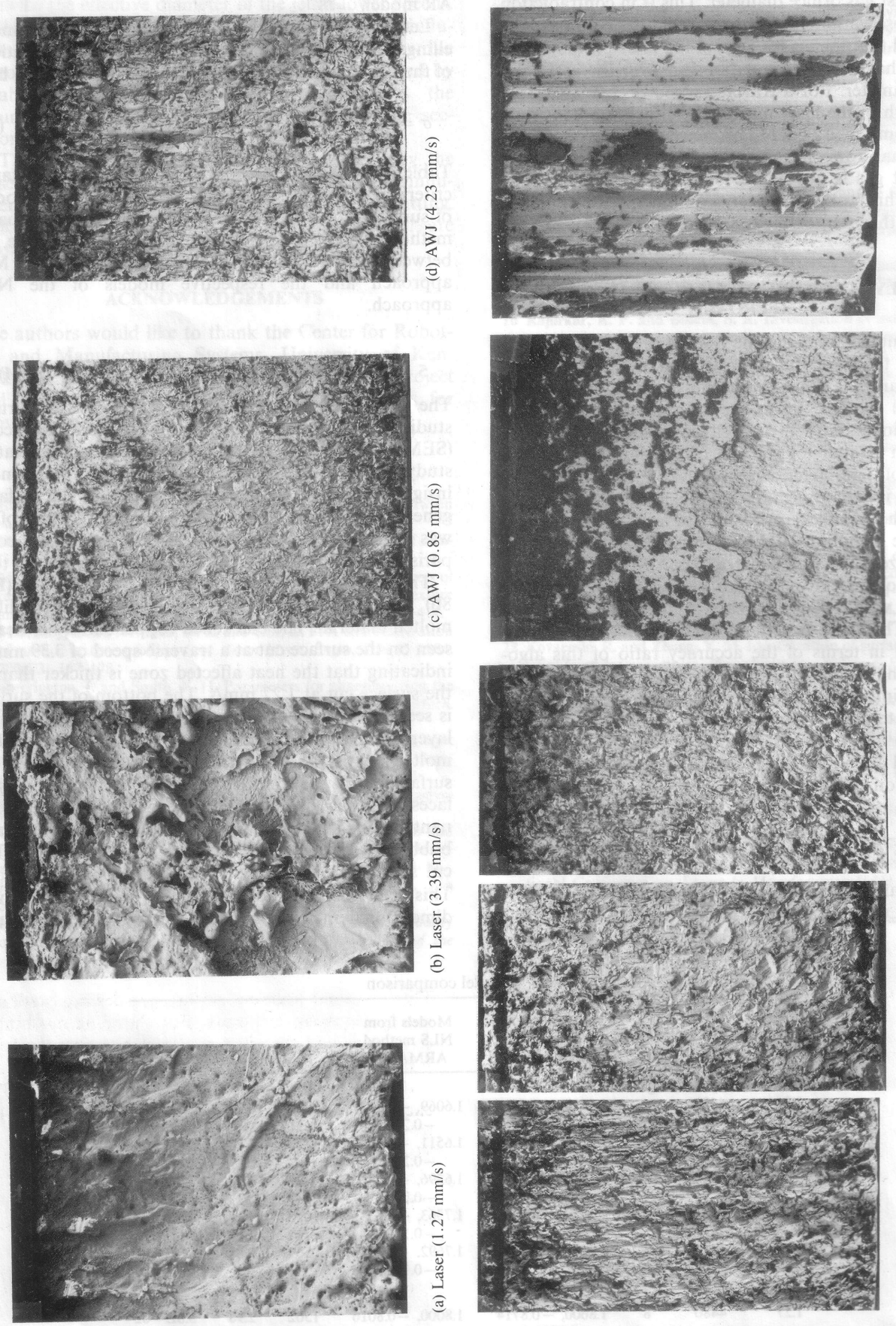

Fig. 8 SEM photographs (magnification × 50)

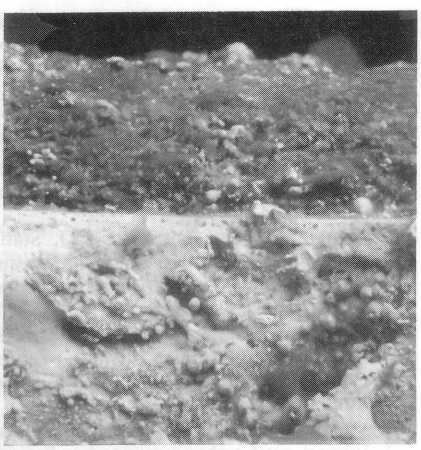

(a) Laser (1.27 mm/s)

(b) Laser (3.39 mm/s)

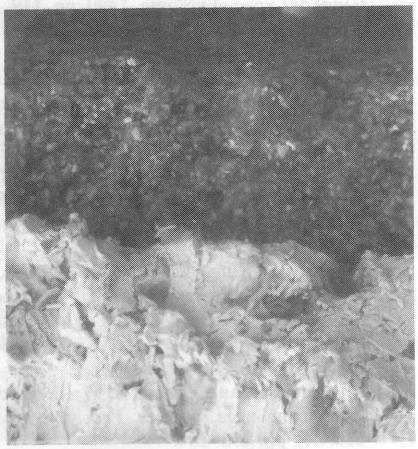

(c) AWJ (44.45 mm/s)

(d) Shearing

Fig. 9 SEM photographs (magnification × 500)

resolidification. To obtain a better idea of the ceramic layer peel-off, the SEM photograph (with magnification × 500) of the ceramic layer–copper interface is taken. From Fig. 9a and b the ceramic layer peel-off at edges is clearly seen for a cutting speed of 3.39 mm/s. These photographs also show the solidified inclusions.

The SEM photographs of the AWJ cut surface (Fig. 8c to g) show that the surface is comparatively much better. Edges are relatively smooth with very little burr (burr is observed only at a cutting speed of 44.45 mm/s). Much less impurities are seen on the surface. No heat affected zone is present. No ceramic layer peel-off is observed. Abrasive grains are found loosely attached to the kerf, but can be removed very easily. Striations are observed along the direction of AWJ flow. A SEM photograph of the ceramic layer–copper interface magnified 500 times is shown in Fig. 9c. This photograph also establishes the fact that ceramic layer peel-off is not present for the AWJ cut.

The SEM photograph of the sheared surface (Fig. 8h) indicates two distinct zones of failure—the fracture zone and the burnished zone. The ceramic layer is crushed at the edges and is peeled off. Burrs are observed at the bottom edge. Top layer particles are seen as inclusions in the sub-surface. Crushed ceramic layer can be seen in the SEM photograph magnified 500 times (Fig. 9d).

The SEM photograph of the bandsaw cut surface (Fig. 8i) shows that the surface is very rough. Heavy burrs are observed at the bottom edge. The cut is not straight. The top ceramic layer is stuck to the copper base. Cut surface orientation is in a direction perpendicular to the direction of cut.

6 CONCLUSIONS

1. The AWJ and laser cut surface profiles are predominantly Gaussian in nature. For the same machining conditions and the given material, the quality of the AWJ cut surface is much better than the laser cut surface. The dynamic response of the system is influenced significantly by the traverse speed (indicated by the trend of variance).
2. System dynamics is reflected on the surface profile. Hence parameters like Green's function and/or power spectrum density which measure the dynamics of the system can be used for surface profile representation.
3. Stochastic modelling is found to be effective in analysing the dynamic response of the system. The model distance based approach is a very useful tool for ARMA identification. This method gives much more accurate ARMA models than the NLS method.
4. Primary and secondary wavelengths are responsible

for the surface profile of AWJ cut surfaces. Jet stream causes the primary wavelength and is approximately twice the effective diameter of the jet at lower speeds. At higher speeds, the primary wavelength is influenced by the reduction in effective jet diameter due to kerf taper. The secondary wavelength is caused by abrasive grains. At higher traverse speeds the unsteadiness of the traverse system affects the secondary wavelength.

5. The type of flow of the laser jet enveloped by the secondary gas is the predominant factor that influences the wavelength of the profile in laser cutting. Reduction in kerf width and kerf width taper are observed at higher traverse speeds.

ACKNOWLEDGEMENTS

The authors would like to thank the Center for Robotics and Manufacturing Systems, University of Kentucky for the financial support in executing this project and Flow International Inc., Kent, Washington, for providing them with the AWJ cutting system.

REFERENCES

1 **King, T. G.** and **Spedding, T. A.** On the relationships between surface profile height parameters. *Wear*, 1982, **83**, 91–108.
2 **Watson, W.** and **Spedding, T. A.** The time series modeling of non-Gaussian engineering processes. *Wear*, 1982, **83**, 215–231.
3 **Mulvaney, D. J., Newland, D. E.** and **Gill, K. F.** A comparison of orthogonal transforms in their application to surface texture analysis. *Proc. Instn Mech. Engrs, Part C*, 1986, **200**(C6), 407–414.
4 **Mulvaney, D. J., Newland, D. E.** and **Gill, K. F.** A characterization of surface texture profiles. *Proc. Instn Mech. Engrs, Part C*, 1986, **200**(C3), 167–178.
5 **Sherrington, I.** and **Smith, E. H.** Parameters for characterizing the surface topography of engineering components. *Proc. Instn Mech. Engrs, Part C*, 1987, **201**(C4), 297–306.
6 **Tan, D. K. M.** A model for the surface finish in abrasive waterjet cutting. Eighth International Symposium on *Jet cutting technology*, England, 9–11 September 1986, paper 31, pp. 309–313.
7 **Hashish, M.** Characteristics of surfaces machined with abrasive-waterjets. *J. Engng Mater. Technol.*, July 1991, **113**, 354–362.
8 **Kovacevic, R., Liaw, H. H.** and **Barrows, J. F.** Surface finish and its relationship to cutting parameters. *Proceedings of Third International Conference on Grinding*, 1988, paper MR88-589, pp. 1–15.
9 **Kovacevic, R.** Surface texture in abrasive waterjet cutting. *The SME's J. of Manufacturing Systems*, 1991, **10**(1).
10 **Kovacevic, R.** and **Beardsley, H. E.** On line monitoring the quality of the surface cut by the abrasive waterjet. *Proceedings of the Fourth International Conference on Grinding*, Dearborn, Michigan, 9–11 October 1990, paper MR90-535, pp. 1–10.
11 **Hunt, D. C., Kim, T. J.** and **Reuber, M.** Surface finish optimization for abrasive waterjet cutting. Ninth International Symposium on *Jet cutting technology*, October 1988, paper C1, pp. 99–112.
12 **Curhan, J., Reuber, M.** and **Kim, T. J.** Force control of surface finish in abrasive waterjet cutting. *Proceedings of the 1989 ASME WAM*, San Francisco, Calif., 10–15 December 1989, Vol. PED41, pp. 31–36 (ASME).
13 **Burnham, C. D.** and **Kim, T. J.** Statistical characterization of surface finish produced by a high pressure abrasive waterjet. *Proceedings of Fifth American Conference on Waterjets*, Canada, 29–31 August 1989, paper 16, pp. 165–175.
14 **Hunt, D. C., Burnham, C. D.** and **Kim, T. J.** Surface finish characterization in machining advanced ceramics by abrasive waterjet. *Proceedings of Fourth American Conference on Waterjets*, Berkeley, Calif., August 1987.
15 **Webb, K. E.** and **Rajurkar, K. P.** Surface characterization of Inconel cut by abrasive waterjet. *Proceedings of CSME Mechanical Engineering Forum*, 1990.
16 **Rajurkar, K. P.** and **Bhatia, S. K.** Investigation of surface characteristics in electrochemical grinding. *ASME manufacturing international '90*, special volume, 1990, pp. 119–124 (ASME).
17 **Williams, R. E.** and **Rajurkar, K. P.** Stochastic modeling and analysis of abrasive flow machining. *J. Engng for Industry*, February 1992, **114**, 74–81.
18 **Williams, R. E.** and **Rajurkar, K. P.** Study of wire electrical discharge machined surface characteristics. In *Computer aided production engineering*, 1991, pp. 127–138 (Elsevier, Amsterdam).
19 **Bedrin, C., Yuan, S. F.** and **Querry, M.** Investigation of surfaces microgeometry in laser cutting. *Ann. CIRP*, 1988, **37**(1).
20 **Olsen, F. O.** Cutting front formation in laser cutting. *Ann. CIRP*, 1989, **38**(1).
21 **Powell, J., King, T. G.** and **Menzies, I. A.** Cut edge quality improvement by laser pulsing. Proceedings of Second International Conference on *Lasers in manufacturing* (*LIM-2*), Birmingham, 1985, pp. 37–45 (IFS (Publications) Ltd, UK, and North-Holland, Amsterdam).
22 **Kovacevic, R.** and **Zhang, Y. M.** Identification of surface characteristics from large samples. *Proc. Instn Mech. Engrs, Part C*, 1992, **206**(C4), pp. 275–284.
23 **Mohan, R., Kovacevic, R.** and **Zhang, Y. M.** Characterization of surface texture generated by high energy jets. *Proceedings of the ASME Winter Annual Meeting*, Anaheim, Calif., 8–13 November 1992, Vol. PED 62, pp. 203–218 (ASME).
24 **Pandit, S. M.** and **Wu, S. M.** *Time series and system analysis with applications*, 1983 (John Wiley, New York).
25 **Box, G. E. P.** and **Jenkins, G. M.** *Time series analysis, forecasting and control*, 1976 (Holden Day, California).
26 **Querry, M., Yuan, S. F.** and **Bedrin, C.** Characterization of surface morphology in laser cutting. Proceedings of the Third International Conference on *Lasers in Manufacturing* (*LIM3*), 3–5 June 1986, pp. 55–66 (IFS (Publications) Ltd, UK).
27 **Hashish, M.** Visualization of the abrasive waterjet cutting process. *Experimental Mechanics*, June 1988, pp. 159–169.